Combined Neutron Diffraction, NMR, and Electrochemical Investigation of the Layered-to-Spinel Transformation in $LiMnO_2$

A. Robert Armstrong,[†] Nicolas Dupre,[‡] Allan J. Paterson,[†] Clare P. Grey,*[,‡] and Peter G. Bruce[†]

School of Chemistry, The Purdie Building, University of Saint Andrews, Fife, KY16 9ST, U.K., and Chemistry Department, State University of New York (SUNY) Stony Brook, Stony Brook, New York 11794-3400

Received October 7, 2003. Revised Manuscript Received May 12, 2004

The conversion that occurs from layered $LiMnO_2$ to spinel on electrochemical cycling has been studied by neutron diffraction and NMR. Neutron diffraction results indicate that the tetrahedral sites in the Li layers that share faces with octahedral sites in the transition metal layers are occupied even following the first charge to 4.6 V. NMR results are consistent with the conversion from the monoclinic, Jahn−Teller distorted, to the rhombohedral, layered phase on charging. On subsequent discharging, clear evidence for the monoclinic phase is seen by NMR indicating the presence of Jahn−Teller distorted domains in the material at 3.5 V and below. The fraction of monoclinic phase decreases gradually as a function of cycle number and disappears by 35 charge−discharge cycles. Diffraction patterns obtained as a function of cycle number were refined with a structural model that included both a layered phase (with octahedral and tetrahedral site occupancy) and a spinel phase, with the fraction of spinel increasing from 0.12 (5 cycles) to 0.93 following 92 cycles. Both diffraction and NMR results indicate that the spinel phase that nucleates from the layered material is stoichiometric and does not contain Li occupancy on the Mn sites. An additional site is seen by NMR which reaches a maximum in cycles 25−50, which is assigned to tetrahedrally coordinated Li in a local environment intermediate between that of the spinel and the layered phase. The observation of this site by NMR is associated with two characteristic peaks in the incremental capacity plot at 3.75 and 3.9 V on charge and discharge. The data indicate that the mechanism for Li insertion and removal into these local environments is complex and involves simultaneous structural rearrangements. The intermediate environment decreases in concentration on subsequent cycling as the concentration of the spinel phase continues to grow.

Introduction

Many intercalation reactions, e.g., Li_xCoO_2, Li_xNiO_2, were originally considered to involve the continuous insertion/removal of guest species into/from a solid host without a change of structure. However, in recent years, it has been demonstrated that the majority of such reactions are not continuous solid solutions spanning a wide composition range but instead pass through a series of different phases as the guest ions are inserted/removed. Indeed it now appears that such behavior is ubiquitous. These structural transformations are in themselves interesting, but they also have important implications for the physical properties, and hence applications of such materials in devices, for example rechargeable lithium batteries.[1−3] There is however another issue which is of great importance in the context of the use of intercalation compounds in electrochemical devices and that is the presence of structural changes on repeated insertion/removal, i.e., on cycling. It is this aspect that concerns us here.

Layered $LiMnO_2$ was first synthesized several years ago.[4,5] Since then it has been shown that the material may be prepared in stoichiometric $LiMnO_2$, or nonstoichiometric $Li_xMn_yO_2$ ($x \approx 0.6$, $y \approx 0.95$) forms.[6−8] Following its initial discovery, interest in the layered lithium manganese oxides, as well as in their derivatives formed by replacement of Mn by other ions, has grown significantly.[9−14] This interest is due to their

* To whom correspondence should be addressed. Tel: 631-632-9548. Fax: 631-632-5731. E-mail: cgrey@notes.cc.sunysb.edu.
[†] University of Saint Andrews.
[‡] SUNY Stony Brook.

(1) Bruce, P. G.; Irvine, J. T. S. In *Encyclopedia of Materials: Science and Technology*; Elsevier: Oxford, 2002.
(2) Tarascon, J.-M.; Armand, M. *Nature* **2001**, *414*, 359.
(3) Bruce, P. G., Ed. *Solid State Electrochemistry*, Cambridge University Press: New York, 1995.
(4) Armstrong, A. R.; Bruce, P. G. *Nature* **1996**, *381*, 499.
(5) Capitaine, F.; Gravereau, P.; Delmas, C. *Solid State Ionics* **1996**, *89*, 197.
(6) Armstrong, A. R.; Gitzendanner, R.; Robertson, A. D.; Bruce, P. G. *Chem. Commun.* **1998**, 1833.
(7) Robertson, A. D.; Armstrong, A. R.; Bruce, P. G. *Chem. Commun.* **2000**, 1997.
(8) Armstrong, A. R.; Paterson, A. J.; Robertson, A. D.; Bruce, P. G. *Chem. Mater.* **2002**, *14*, 710.
(9) Armstrong, A. R.; Robertson, A. D.; Gitzendanner, R.; Bruce, P. G. *J. Solid State Chem.* **1999**, *145*, 549.

10.1021/cm034964b CCC: $27.50
Published on Web 07/08/2004

potential use as low cost, low toxicity, safe, and high capacity (200 $mAhg^{-1}$ at a rate of 25 mAg^{-1}) positive electrodes in rechargeable lithium batteries.[7,10−12] The structures of stoichiometric and nonstoichiometric layered lithium manganese oxides may be described as close-packed oxide ion layers stacked in an ABC sequence (cubic close packing) with alternate sheets of octahedral sites between the oxide ion layers being occupied by Li and Mn (the sites are fully occupied in the case of stoichiometric $LiMnO_2$ but exhibit vacancies in the Li and Mn sites for the nonstoichiometric materials).[4,8,10]

It is known that on removal of Li (specifically at the $Li_{0.5}MnO_2$ composition) the layered structure begins to convert to that of spinel, which possesses the same stacking of oxide ions.[15,16] The structural reorganization therefore involves only a redistribution of the cations. It might have been expected that such a structural reorganization would have profoundly detrimental effects on the ability to remove and reinsert lithium and hence in the operation of such an intercalation compound as an electrode in rechargeable lithium batteries. A number of authors have discussed the need to avoid the layered-to-spinel transformation and hence retain a layered structure on cycling.[17,18] In fact the spinel that forms on cycling demonstrates far superior capacity retention when cycled over a wide composition range compared with that of directly prepared spinel. Whereas the latter can achieve only 120 $mAhg^{-1}$ without significant capacity fade, the spinel formed in situ exhibits a capacity of 200 $mAhg^{-1}$ at 25 mAg^{-1}, fading by less than 0.08% per cycle at room temperature.[10−12] The ability of our materials to demonstrate excellent cyclability over a wide composition range, once converted to a spinel structure, has been investigated and it has been shown that the origin of this lies in the formation of a nanodomain structure within the micrometer-sized particles in the electrode. Such a nanostructure appears to be able to accommodate the strain of the Jahn−Teller driven phase transformation that accompanies cycling the spinel over a wide composition range ($Li_xMn_2O_4$, $0 < x < 2$), with the strain being accommodated by slippage at the domain wall boundaries. This provides a means of circumventing the long standing problem of capacity fade related to the cubic/tetragonal phase transformation on cycling.[15,19−22]

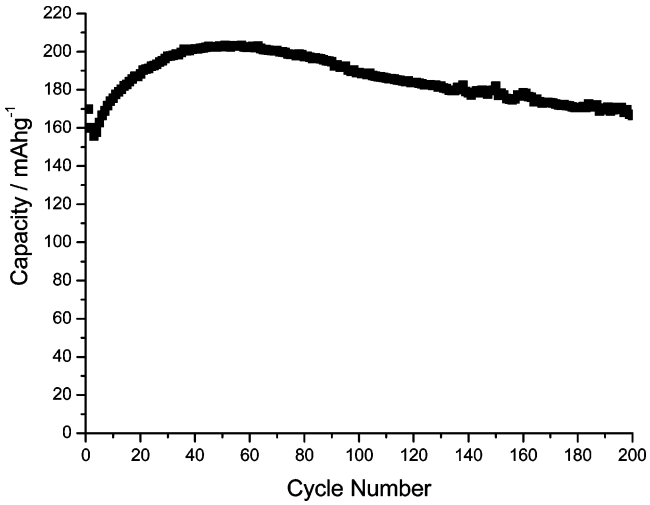

Figure 1. Discharge capacity as a function of cycle number for stoichiometric $LiMnO_2$ at 30 °C. Rate = 25 mAg^{-1} (approximately C/8). Voltage limits = 2.5−4.6 V.

Although once converted to a spinel phase the cyclability is excellent, this is not always so during conversion. While nonstoichiometric, especially doped, materials can exhibit only a minor drop in capacity of <5%, recovering thereafter, others of the layered family can suffer more significantly on passage from the layered to the spinel structure. This is particularly true for stoichiometric $LiMnO_2$ as shown in Figure 1. Here we carry out an investigation of how the stoichiometric layered $LiMnO_2$ converts to spinel.

The transformation from a layered to spinel structure will involve local rearrangements of ions as well as the nucleation and growth of well-defined phases. As a result, it is important to follow these changes with techniques that probe short and long-range structure. We have selected magic angle spinning NMR as a probe of the local structure. One of us has carried out extensive investigation of Li NMR in lithium manganese oxide compounds and as a result has determined the shifts expected for various lithium environments in these materials.[23,24] The long-range structure is probed by diffraction.

Because Li is a weak scatterer of X-rays it is advantageous to employ neutron powder diffraction for the investigation of long range structure in lithium compounds. Conventionally the application of such a technique has required samples in excess of 0.5−1 g. Although it is not impossible to cycle electrochemical cells with electrodes of this quantity, it is not feasible to achieve high cycle numbers at comparable rates and in similar time scales in small cells. The advent of a new generation of high-intensity neutron powder diffractometers, with high detector area, such as GEM at the ISIS facility, Rutherford Appleton Laboratory, represents a significant breakthrough in the study of intercalation electrodes. It is now possible to obtain high-quality neutron powder diffraction data on samples

(10) Robertson, A. D.; Armstrong, A. R.; Fowkes, A. J.; Bruce, P. G. *J. Mater. Chem.* **2001**, *11*, 113.
(11) Quine, T. E.; Duncan, M. J.; Armstrong, A. R.; Robertson, A. D.; Bruce, P. G. *J. Mater. Chem.* **2000**, *10*, 2838.
(12) Robertson, A. D.; Armstrong, A. R.; Paterson, A. J.; Duncan, M. J.; Bruce, P. G. *J. Mater. Chem.* **2003**, *13*, 2367.
(13) Ammundsen, B.; Desilvestro, J.; Groutso, T.; Hassell, D.; Metson, J. B.; Regan, E.; Steiner, R.; Pickering, P. J. *J. Electrochem. Soc.* **2000**, *147*, 4078.
(14) Davidson, I. J.; McMillan, R. S.; Slegr, H.; Luan, B.; Kargina, I.; Murray, J. J.; Swainson, I. P. *J. Power Sources* **1999**, *81−82*, 406.
(15) Bruce, P. G.; Armstrong, A. R.; Gitzendanner, R. L. *J. Mater. Chem.* **1999**, *9*, 193.
(16) Armstrong, A. R.; Robertson, A. D.; Bruce, P. G. *Electrochim. Acta* **1999**, *45*, 285.
(17) Ammundsen, B.; Paulsen, J. *Adv. Mater.* **2001**, *13*, 943.
(18) Paulsen, J. M.; Thomas, C. L.; Dahn, J. R. *J. Electrochem. Soc.* **1999**, *146*, 3560.
(19) Jang, Y.-I.; Huang, B.; Chiang, Y.-M.; Sadoway, D. R. *Electrochem. Solid-State Lett.* **1998**, *1*, 13.
(20) Wang, H.; Jang, Y.-I.; Chiang, Y.-M. *Electrochem. Solid-State Lett.* **1999**, *2*, 490.
(21) Chiang, Y.-M.; Wang, H.; Jang, Y.-I. *Chem. Mater.* **2001**, *13*, 53.
(22) Shao-Horn, Y.; Hackney, S. A.; Armstrong, A. R.; Bruce, P. G.; Gitzendanner, R.; Johnson, C. S.; Thackeray, M. M. *J. Electrochem. Soc.* **1999**, *146*, 2404.
(23) Lee, Y. J.; Wang, F.; Grey, C. P. *J. Am. Chem. Soc.* **1998**, *120*, 12601.
(24) Lee, Y. J.; Wang, F.; Mukerjee, S.; McBreen, J.; Grey, C. P. *J. Electrochem. Soc.* **2000**, *147*, 803.

of no more than a few tens of mg, in a few hours. This facility has been extensively employed in the present work.

In this paper we examine the structural evolution, from layered to spinel, of stoichiometric $LiMnO_2$ on subjecting the material to 92 charge/discharge cycles.

Experimental Section

Stoichiometric $NaMnO_2$ materials were prepared by solid-state reaction between Na_2CO_3 (Aldrich 99.5+%) and Mn_2O_3 (Aldrich 99+%) in mole ratios corresponding to Na/Mn = 1.05. The powdered samples were fired at 720 °C under flowing argon for up to 24 h. The sodium phase was then ion exchanged under reflux in hexanol at 160 °C with a 7−8-fold molar excess of LiBr for up to 2 weeks. The resulting materials were washed with ethanol and dried overnight. Chemical analyses for sodium and lithium were carried out by flame emission and for manganese using atomic absorption spectroscopy. The average manganese oxidation state was determined by redox titration using ferrous ammonium sulfate/$KMnO_4$.[25]

Powder X-ray diffraction data were collected on a Stoe STADI/P diffractometer operating in transmission mode with Fe $K\alpha_1$ radiation (λ = 1.936 Å). Compounds of manganese exhibit fluorescence when irradiated by copper X-ray radiation. Although this may be eliminated by using an analyzing monochromator between the sample and the detector, such an approach precludes the use of a primary beam monochromator. By using an iron source with a curved germanium monochromator and a small angle position sensitive detector operating in transmission mode, excellent data may be obtained from Mn containing samples.

To prepare the electrochemically cycled materials for characterization by neutron diffraction and solid-state NMR, composite electrodes were constructed by mixing the active material, carbon, and Kynar Flex 2801 (a copolymer based on PVDF) in the weight ratio 85:10:5. The mixture was prepared as a slurry in THF and spread onto aluminum foil using a doctor blade technique. Following evaporation of the solvent and drying, electrodes were incorporated into an electrochemical cell with a lithium metal counter electrode and the electrolyte was a 1 molal solution of $LiPF_6$ in ethylene carbonate/dimethyl carbonate (1:1) (Merck). Electrochemical measurements were carried out using a Biologic MacPile II. Typically cells were cycled between 2.5 and 4.6 V at rates of around 25 $mAhg^{-1}$. After cycling, the Kynar was dissolved and the samples were centrifuged before they were dried and loaded into capillaries.

An additional series of samples enriched in ^6Li was prepared for the ^6Li NMR experiments by using ^6Li-enriched Li metal as the anode. An aluminum disk was coated with a slurry made by adding cyclopentanone to a mixture composed of 80% active material and 20% acetylene black carbon, and drying under vacuum at ambient temperature for a few hours. A 1 M $LiPF_6$ solution in ethylencarbonate/dimethyl carbonate (EC/DMC, Merck) was used as electrolyte. The cells were assembled in an argon atmosphere. Samples were stabilized electrochemically, after galvanostatic cycling, using the potentiodynamic mode with Li metal as the counter/ reference electrode. A cycling rate of C/20 (10 mAg^{-1}) was used (calculated based on the maximum theoretical capacity of $LiMnO_2$). Samples were equilibrated at potentials corresponding to different steps of the intercalation/deintercalation process. A range of potentials was chosen so that all major processes were monitored. The cells were then disassembled and the cathodes were washed with EC/DMC to remove residual electrolyte before packing the samples in NMR rotors in an inert atmosphere for the NMR experiments.

Time-of-flight powder neutron diffraction data on the cycled materials were obtained on the new GEM diffractometer at ISIS at the Rutherford Appleton Laboratory. The samples were contained in 2-mm quartz capillaries. The structures were refined by the Rietveld method using the program Prodd based on the Cambridge crystallographic subroutine library (CCSL).[26,27] Scattering lengths of −0.19, −0.373, and 0.5803 (all × 10^{-12} cm) were assigned to Li, Mn, and O, respectively.[28] Lattice parameters were obtained from X-ray diffraction data by Rietveld refinement using GSAS.[29]

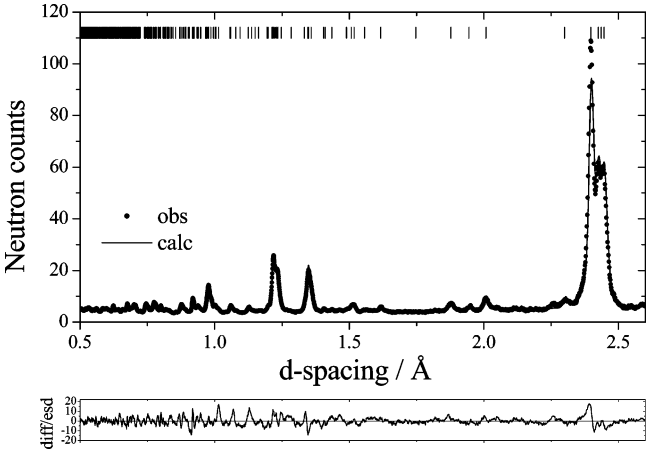

Figure 2. Refined powder neutron diffraction pattern for as-prepared $LiMnO_2$. Dots represent observed data and solid line represents the calculated pattern. The lower line is the difference/esd.

^6Li and ^7Li magic angle spinning (MAS) NMR experiments were run on the same samples used in the diffraction experiments. Additional ^6Li NMR spectra were acquired from the cathode materials cycled with the ^6Li anode. Experiments were performed at operating frequencies of 29.47 and 77.79 MHz, for ^6Li and ^7Li, respectively, on a CMX-200 spectrometer. Spectra with spinning frequencies (ν_r) of less than 20 kHz were acquired with a Chemagnetics probe equipped with a 3.2-mm rotor, while spinning frequencies of 40 kHz were achieved by using a fast MAS, 2-mm probe, built by A. Samoson and coworkers. All spectra were acquired with a rotor synchronized echo sequence (90°−τ−180°−τ−acq.), where $\tau = 1/\nu_r$. $\pi/2$ pulse widths of 2.8 μs for ^6Li on the CMX-200 spectrometer and 2.1 μs for ^7Li on the CMX-200 spectrometer were used with pulse delays of 0.2−0.5 s. "Room temperature" (i.e., a spectrum acquired with no control of the temperature) corresponds to a sample temperature of between 70 and 80 °C. The sensitivity of the ^7Li nucleus is considerably higher, allowing spectra from a wider range of materials to be acquired. Some of these cathode materials were then probed by using ^6Li MAS NMR, since higher resolution spectra may be typically obtained from this nucleus. Spin−lattice relaxation times (T_1) were measured using an inversion−recovery sequence (180°−τ_D−90°−acq.), where τ_D is a delay under our control.

Results and Discussion

A fitted neutron powder diffraction pattern for the as-prepared $LiMnO_2$ material is shown in Figure 2. This is in good agreement with the pattern published previously.[4] A model based on the structure of the parent $NaMnO_2$ phase was used as a basis for the Rietveld refinement. The structure consists of close packed oxide ion layers stacked in an ABC sequence with alternate sheets of octahedral sites occupied by Li and Mn.

(25) Katz, M. J.; Clarke, R. C.; Nye, W. F. *Anal. Chem.* **1956**, *28*, 507.

(26) Matthewman, J. C.; Thompson, P.; Brown, P. J. *J. Appl. Crystallogr.* **1982**, *15*, 167.

(27) Brown, P. J.; Matthewman, J. C. Rutherford Appleton Laboratory Report, RAL-87-010, 1987.

(28) Sears, V. F. *Neutron News* **1992**, *3* (3), 26.

(29) Larson, A. C.; von Dreele, R. B. General Structure Analysis System, Los Alamos National Laboratory: Los Alamos, NM, 1995.

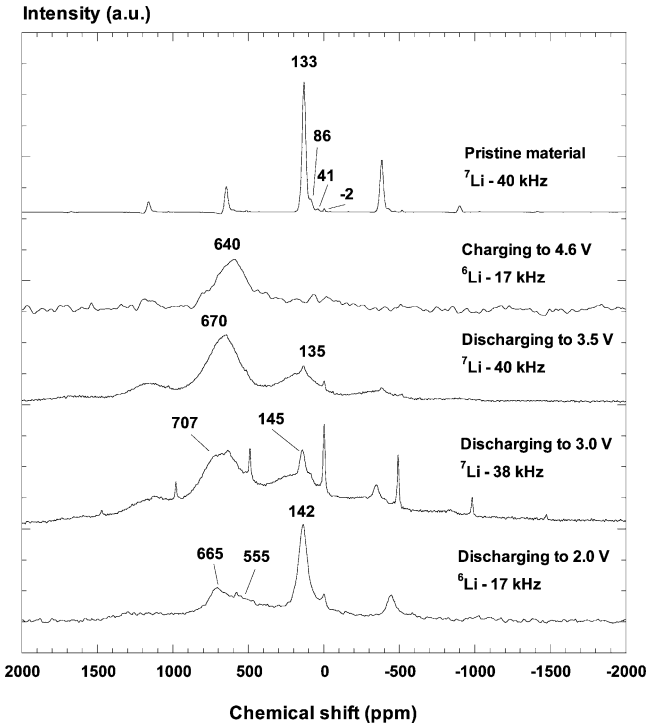

Figure 3. Lithium (^{6}Li and ^{7}Li) NMR of $LiMnO_2$ in the first cycle. The spinning speeds used to acquire the spectra are marked. The isotropic resonances are labeled with their corresponding shifts; the remaining peaks are spinning sidebands. The intense resonance at 0 ppm is due to lithium salts in the electrolyte.

Although the structure is essentially that of $LiCoO_2$ (α-$NaFeO_2$ type), the presence of the Jahn−Teller active high spin $3d^4$ Mn^{3+} ion distorts the structure and lowers the space group symmetry from $R\bar{3}m$ to $C2/m$. Lattice parameters obtained from the refinement were a = 5.447(2) Å, b = 2.8085(1) Å, c = 5.399(2) Å, β = 116.069(8)°, with R-factors R_e = 0.90%, R_{wP} = 3.47%, R_P = 5.79% (χ^2 = 14.8). The occupancies of the transition metal and alkali ion sites were refined and found to be, respectively, 0.98(4) and 0.92(4), in excellent agreement with the values derived from chemical analysis of 0.99 (Mn) and 0.91 (Li). The ^{7}Li MAS NMR of the same material is consistent with this structural model (top spectrum; Figure 3). The spectrum is dominated by a resonance at 133 ppm, which is assigned to lithium in the monoclinically distorted layered phase. Three very weak resonances are seen at 86, 41, and −2 ppm. The lower frequency resonance is assigned to the orthorhombic phase of $LiMnO_2$ (*o*-$LiMnO_2$; 41 ppm),[30] while the resonance at −2 ppm is due to diamagnetic impurities such as lithium carbonate. The resonance at 86 ppm is tentatively assigned to defects in the layered material, which result in local environments for Li that are intermediate between the layered and orthorhombic phases. Similar defects have been observed for *o*-$LiMnO_2$.[31]

The incremental capacity plots collected on cycling a cell containing a $LiMnO_2$ electrode at 25 mAg^{-1}, between potential limits of 2.5−4.6 V versus Li^+ (1M)/Li, are shown in Figure 4. We have reported previously that on first extracting Li from layered $LiMnO_2$, a two-phase region exists between rhombohedral $Li_{0.5}MnO_2$ and monoclinic $LiMnO_2$.[15] This is associated with a peak at 3.3 V on the first charge in Figure 4. A peak at 4 V in such plots is normally taken to indicate the presence of Li ions in tetrahedral sites. The 4 V peak on charging may be associated with this but as we shall discuss later such an interpretation is probably too simplistic in the present case.

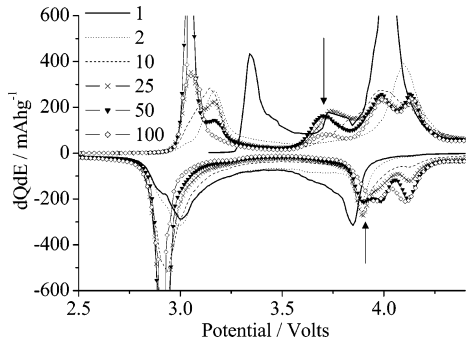

Figure 4. Incremental capacity plots for stoichiometric $LiMnO_2$ as a function of cycle number. Cycling was performed at 25 mAg^{-1} (approximately C/8). T = 30 °C. The 3.75 V oxidation and 3.9 V reduction processes seen in intermediate cycles are marked with arrows.

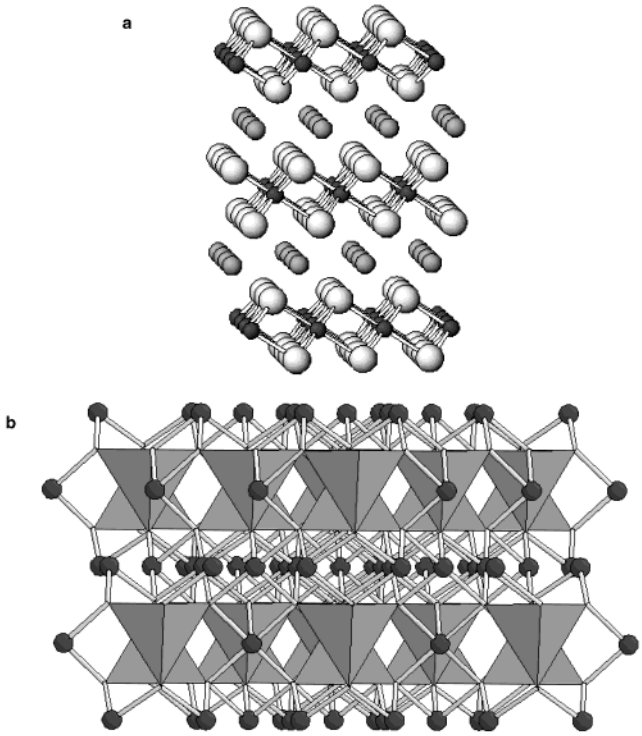

Figure 5. (a) View of layered $LiMnO_2$ structure: dark gray, Mn; gray, Li; white, O. (b) View of $LiMn_2O_4$ spinel structure emphasizing layers: dark gray, Mn; gray, tetrahedral cation sites.

The layered and spinel structures are compared in Figure 5 where both structures are presented with their close-packed oxygen layers in the same orientation. We know that transformation from the spinel structure ultimately occurs on cycling and that this must involve 25% of the Mn ions migrating from the octahedral sites in the Mn layer into octahedral sites in the Li layers, with the octahedrally coordinated Li ions in these layers being displaced to tetrahedral sites. How might this migration occur? The layered structure consists of

(30) Lee, Y. J.; Grey, C. P. *Chem. Mater.* **2000**, *12*, 3871.
(31) Lee, Y. J.; Grey, C. P.; Deniard, P. Unpublished results.

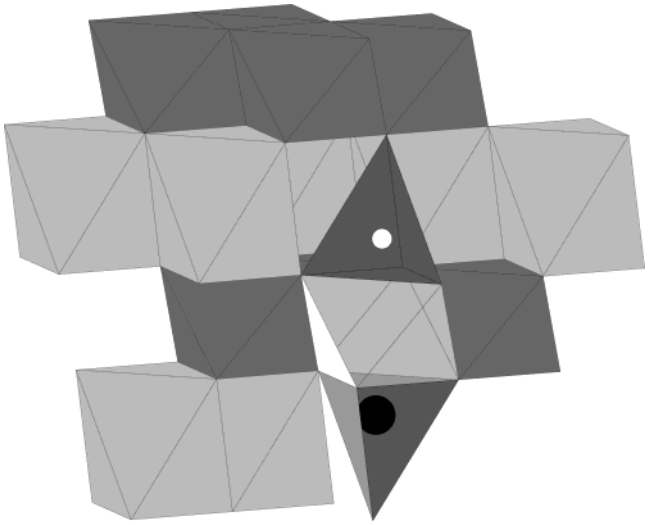

Figure 6. View of layered $LiMnO_2$ structure: LiO_6 octahedra, light gray; MnO_6 octahedra, dark gray; MO_4 tetrahedra, dark gray; Li, white; Mn, black; octahedron around vacant Mn, pale gray.

sheets of MnO_6 octahedra sharing common edges alternating with sheets of LiO_6 octahedra, which also share common edges. Within the Mn layers, the MnO_6 octahedra are bridged by empty tetrahedral sites with which they share faces. A similar situation pertains within the Li layers with empty tetrahedral sites sharing faces with LiO_6 octahedra. Furthermore, the MnO_6 octahedra in the Mn layer share faces with the empty tetrahedral sites in the LiO_6 layers located immediately above and below the Mn layers. Again, the corresponding situation occurs for the LiO_6 octahedra in the Li layers. Mn ions can migrate through a common face into the empty tetrahedral sites in the Li layers when the lithium content is reduced to 50% ($Li_{0.5}MnO_2$), since it is then possible for the rest of the lithium ions in the Li layers to avoid the three octahedral sites in these layers which share faces with the now-occupied tetrahedral site. Such a Mn_{tet} with three neighboring vacant Li_{oct} sites in the Li layer constitutes a defect in the normal layered structure. Following this Mn displacement, there is now a vacant MnO_6 site in the Mn layer and it is possible to displace a Li ion from its octahedral site, through a shared face, into a neighboring tetrahedral site in the Li layer, since there is no longer an unfavorable face-sharing interaction with a Mn ion. Hence, Li and Mn may occupy tetrahedral sites forming a slightly more complex defect than that described above (Figure 6). Reed, Ceder, and van der Ven have investigated the layered-to-spinel transformation using computational methods (density functional theory).[32] They have proposed a transformation mechanism that is very similar to that suggested above, but that involves two distinct stages. The first stage involves displacement of a Mn ion from an octahedral to a tetrahedral site in the neighboring lithium layer with a lithium ion in the other adjacent layer migrating from an octahedral site into the tetrahedral site which shares a face with the now vacant Mn site. As a consequence each pair of tetrahedral Li and Mn ions form a "dumb-bell" with the empty octahedral Mn site in the middle. A structure with such

(32) Reed, J.; Ceder, G.; van der Ven, A. *Electrochem. Solid-State Lett.* **2001**, *4*, A78.

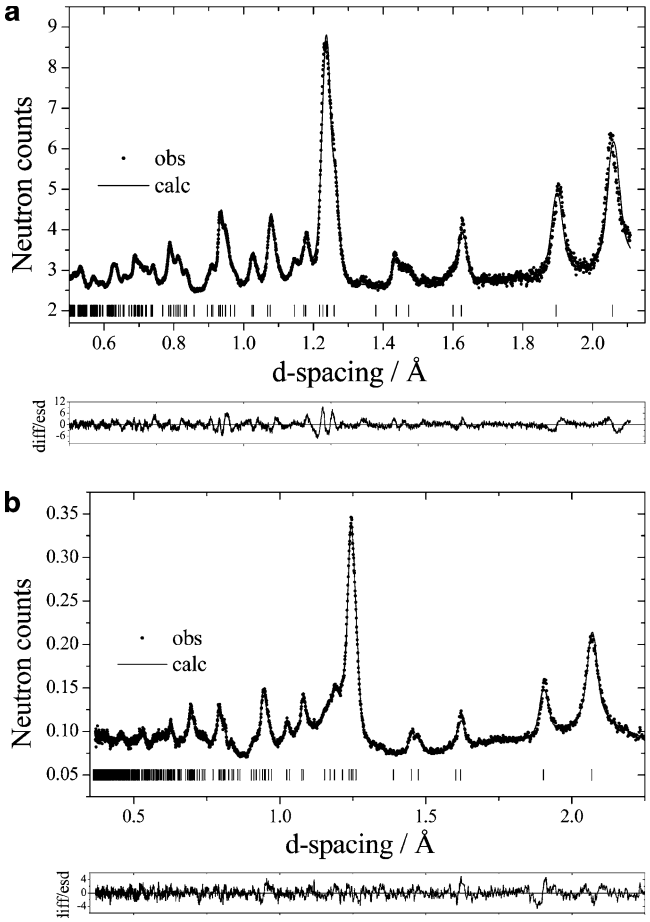

Figure 7. (a) Refined powder neutron diffraction pattern for layered $LiMnO_2$ charged to 4.0 V. (b) Refined powder neutron diffraction pattern for layered $LiMnO_2$ on the first discharge at 3.0 V. Dots represent observed data and solid line represents the calculated pattern. The lower line is the difference/esd.

an arrangement has been referred to as "splayered" (i.e., intermediate between a layered and a spinel phase). Following this first stage, a further, correlated, rearrangement of Li and Mn ions is thought to occur to form the spinel structure. Reed et al. have shown that the first process is relatively facile, whereas the second is more energetically demanding, involving the nucleation and growth of spinel.[32]

We have investigated experimentally the possibility of tetrahedral site occupancy within the layered phase. We have not restricted our attention to a model with equal proportions of tetrahedral Li and Mn. In this paper, when we refer to a splayered phase we imply that Mn exists in tetrahedral sites in the Li layers, but Li may be in either octahedral sites or in both octahedral and tetrahedral sites. We also allow the possibility of Mn being in octahedral sites in the lithium layers.

The First Cycle. Neutron powder diffraction data were collected on the material charged to 4 V on the first cycle, Figure 7a. The data were indexed on a rhombohedral cell, $R\bar{3}m$ with $a = 2.8701(5)$ Å, $c = 14.6134(17)$ Å. Rietveld refinement was based on the normal layered structure, i.e., undistorted α-$NaFeO_2$ ($LiCoO_2$) with Mn occupying the octahedral 3a sites in the transition metal layers and Li occupying the octahedral 3b sites in the alkali metal layers. Refinement of this structural model, allowing freely varying occupancies of the octahedral sites, provided a reasonable

Table 1. Refined Crystallographic Parameters for $Li_{0.5}MnO_2$ (a) on First Charge, Splayered Model, and (b) on First Discharge, Splayered Model

atom	Wyckoff symbol	*x*/*a*	*y*/*b*	*z*/*c*	B_{iso}	occupancy
(a) First Charge, Splayered Model[a]						
Li1	3b	0	0	0.5	1.0(−)	0.37(2)
Li2	6c	0	0	0.1134(14)	0.5(−)	0.160(9)
Mn1	3a	0	0	0	*c*	0.95(2)
O1	6c	0	0	0.26248(12)	*d*	1
(b) First Discharge, Splayered Model[b]						
Li1	3b	0	0	0.5	1.0(−)	0.30(3)
Li2	6c	0	0	0.123 (2)	0.5(−)	0.209(12)
Mn1	3a	0	0	0	0.87(10)	0.95(2)
O1	6c	0	0	0.2612(2)	1.23(5)	1

[a] $a = 2.8701(5)$ Å, $c = 14.6134(17)$ Å. $R_e = 1.12\%$, $R_{wP} = 2.08\%$, $R_P = 2.31\%$, $\chi^2 = 3.45$. [b] $a = 2.9001(7)$ Å, $c = 14.5703(24)$ Å. $R_e = 2.30\%$, $R_{wP} = 2.93\%$, $R_P = 2.42\%$, $\chi^2 = 1.62$. [c] $B_{11} = B_{22} = 1.21(8)$, $B_{33} = 1.18(11)$, $B_{12} = 0.61(4)$. [d] $B_{11} = B_{22} = 1.52(4)$, $B_{33} = 0.77(4)$, $B_{12} = 0.76(2)$.

fit; however, on introducing lithium into the tetrahedral 6c site and permitting its occupancy to vary, a significant improvement in the fit was obtained, corresponding to a reduction in χ^2 of 10%. The final refined crystallographic parameters for the structure are given in Table 1a.

Note that all the tetrahedral sites in $R\bar{3}m$ are equivalent and include the tetrahedral sites in the Mn and Li layers. We recognize that the layered-to-spinel transformation is unlikely to involve the tetrahedral sites in the Mn layers because of unfavorable repulsion with octahedral Mn, hence the observed tetrahedral 6c site occupancy will be confined to the tetrahedral sites in the lithium layers. The presence of scattering on the tetrahedral 6c sites indicates that the transformation from the normal layered structure has commenced even on the first charge, consistent with previous studies.[15] Neutron diffraction measures the total scattering from a site. When a site is occupied by two or more ions it is not possible to distinguish between their respective contributions to the total occupancy by refinement. We introduced Li into the tetrahedral 6c site as a probe of the occupancy of this site. Recalling the mechanism of transformation to spinel described above, it is possible that Li and Mn occupy the tetrahedral, 6c, sites and for the same reason may both occupy the octahedral, 3b, sites in the alkali metal layers. Although we cannot determine directly the relative occupancies of the 6c and 3b sites by Li and Mn we may draw some conclusions based on the following. Table 1(a) indicates that 0.05 of the Mn 3a sites are vacant. (We take 2 esds as the range within which values are likely to fall). If these have migrated entirely onto the 6c sites then, given that this site has twice the multiplicity compared with 3a, the occupancy of the 6c by Mn would be 0.025. Because the Mn scattering length is twice that of Li, 0.025 Mn would correspond to an apparent Li occupancy of 0.05. The total 6c site occupancy is 0.16 therefore the actual Li site occupancy would be 0.11 (model 1). If 0.10 Mn were displaced (i.e., −3 esd's), then there are now 0.05 Mn and 0.06 Li on the 6c site (model 2), which is close to the 1:1 ratio of Mn:Li in tetrahedral sites suggested previously by Reed et al.[22] In model 1, the number of vacancies on the 3a site is less than the occupancy of the 6c site, implying that some unfavorable, short 3a−6c site contacts are present. Assuming ordering of the vacancies nearby the 6c Mn/Li ions, these are not present in model 2, suggesting that the errors in the site occupancies may be larger than implied by the esd's. The overall Li content derived from the diffraction data varies from 0.49 to 0.59, depending on the model, in agreement with the content expected based on the charge extracted.

Both octahedral and tetrahedral Li are present in the material charged to 4 V. Normally the highest energy, octahedral (3 V) Li would be removed completely before extracting Li from the lower energy tetrahedral (4 V) sites, yet Li is being removed at 4 V while octahedral Li persists. One explanation may be that once the structural transformation has commenced, especially if some Mn had migrated into the octahedral 3b sites in the alkali metal layers, the octahedral Li ions may be less mobile, leading to preferential extraction of tetrahedral Li. However, examination of Figure 4 indicates that only a small proportion of the Li removed at 4 V is reinserted at this potential on subsequent discharge. Considering the behavior on charge and discharge together, it is more likely that the observed potential on the first cycle reflects the energetics involved in the structural reorganization taking place in the material, and clearly demonstrated by the neutron diffraction data, rather than individual site energies per se. Hence, we do not associate the broad peak at 4 V on charge and the corresponding peak at 3.85 V on discharge as simply arising from removal and reinsertion of Li from tetrahedral sites.

Neutron powder diffraction data were collected on the first discharge at 3.0 V, Figure 7b. The data were well described by $R\bar{3}m$ symmetry, $a = 2.9001(7)$ Å, $c = 14.5703(24)$ Å. Again, attempts to fit a simple layered model to the data were improved by the introduction of tetrahedral site occupancy, which gave a χ^2 of 5.8, 14% lower than with the simple model. Refinement involved variation of occupancies on the 3a, 3b, and 6c sites and the final crystallographic parameters are listed in Table 1b. The structure is rather similar to that obtained on the first charge. In neither case was it possible to detect the presence of a separate spinel phase. The neutron diffraction data are consistent with a single-layered phase containing a random distribution of Li and Mn in tetrahedral sites (although some clustering on the short range is of course possible). Reed et al. suggested that the tetrahedral Li and Mn could ultimately coalesce to form a discrete phase.[32] However, we see no evidence for this in our diffraction data during the first cycle, or on further cycling as shown later.

The results of the lithium NMR measurements on the first charge and discharge are shown in Figure 3. They are consistent with the passage from a layered monoclinic to a layered rhombohedral structure on charging. The spectra (in this figure and shown in later figures) were acquired at a variety of spinning speeds to minimize overlap between the isotropic resonances and the sidebands of the electrolyte peak. On charging to 4.6 V, a weak signal at 640 ppm is obtained due to the relatively small amount of Li that still remains in the material. This resonance shifts slightly to higher frequency (670 ppm) on discharging to 3.5 V, and the resonance due to monoclinic $LiMnO_2$ (135 ppm) starts to emerge.

The large shifts seen in the NMR spectra are due to transferred hyperfine interactions between the Li nuclei and the unpaired electrons of the manganese ions, which are mediated via the intervening oxygen atoms. On the basis of earlier work in the literature, hyperfine shifts of between 500 and 900 ppm are expected for lithium in tetrahedral and octahedral sites in layered materials with manganese oxidation states of 3.5 and above; i.e., in environments near manganese ions that have not undergone a Jahn−Teller distortion.[23,30,33,34] Although the assignments are not always definitive, some general trends have emerged for Li in Mn oxide spinels: the ^{6}Li/^{7}Li hyperfine shifts for Li ions in tetrahedral environments in spinel structures vary from 500 to 900 ppm, with higher and lower shifts being observed for manganese average oxidation states of 3.5 and 4, respectively. Li ions in octahedral environments are generally associated with larger shifts, but the exact values will depend on the numbers and arrangements of nearby Mn ions. Thus, the resonances observed here at 640−670 ppm are consistent with octahedral and tetrahedral Li environments in the lithium layers of Li_xMnO_2 near manganese with an average oxidation state of 3.5+ or higher, the diffraction results indicating that we cannot assign these resonances to either octahedral or tetrahedral Li alone. In previous work, many of the NMR shifts seen in similar materials could be further analyzed by quantifying the number of Mn ions in the 1st and 2nd cation coordination shells and their associated Li−O−Mn bond angles.[35,36] The Li in a tetrahedral site in the Li layers, proposed by Reed et al.,[32] that shares a face with a vacant MnO_6 octahedron in the Mn layers, has a local environment very similar to that found in a spinel, but contains only 9 Li−O−Mn interactions, each with bond angles of approximately 122° (Figure 6), instead of the 12 found for Li in $LiMn_2O_4$. This local environment is analogous to that of the Li ions in the tetrahedral sites of ordered Mn(IV) spinel $(Li_{0.5}Zn_{0.5})_{tet}(Li_{0.5}Mn_{1.5})_{oct}O_4$ where a shift of 688 ppm was observed for this site.[36] Smaller shifts are expected for local environments with increased numbers of Mn^{3+} ions. For example, based on the shift seen for $LiMn_2O_4$ (approximately 512 ppm), a shift of 384 ppm is predicted for Li connected to only 9 Mn ions with an average oxidation state of 3.5. The observed shifts are not consistent with this last environment, indicating that the tetrahedral Li ions present in the sample discharged to 3.5 V are near Mn ions with an oxidation state of >3.5+ or that they must also be near additional Mn ions in the Li layers. The first suggestion is consistent with the model of Reed et al.,[32] where a Mn^{2+} ion is present in the tetrahedral site of the dumb-bell, resulting in a Mn^{4+} ion in the Mn layer. The latter suggestion could occur if some of the Mn displaced from the 3a sites migrates into the octahedral 3b sites in the Li layer. Most likely, both phenomena are occurring.

On discharging to 3.0 V, the broad peak shifts to higher frequency (707 ppm) and the *m*-$LiMnO_2$ resonance (now at 145 ppm) grows in intensity, indicating the formation of domains of ordered $LiMnO_2$, which are large enough to undergo a cooperative Jahn−Teller distortion. A small shift in frequency of the *m*-$LiMnO_2$ resonance from 135 (3.5 V) to 143 ppm (3 V) is seen. A similar shift has been observed on Cr^{3+}-doping of $LiMnO_2$, where the positive shift was ascribed to a reduction in the short-range antiferromagnetic couplings between the Mn^{3+} ions caused by the disorder.[34] The presence of disorder is consistent with the persistence of the resonances above 500 ppm, even for the sample discharged to 2 V, indicating that Mn^{4+} ions and non-Jahn Teller distorted Mn^{3+} ions remain. The 707−765 ppm resonances are assigned to Li in octahedral sites in the rhombohedral layered phase.

There is good agreement between the NMR and neutron data, in that both indicate transformation to a layered rhombohedral structure on charging, which persists on subsequent discharge. The NMR data suggest the presence of some *m*-$LiMnO_2$ phase at 3.5 V (<5%), whereas no such phase was apparent in the diffraction data. Because NMR is a local probe, the peak at 135 ppm indicates that locally some Li ions are surrounded by Jahn−Teller distorted Mn^{3+} ions in an otherwise rhombohedral phase. However, at the lower voltages *m*-$LiMnO_2$ may form as a discrete phase and there is evidence of this in X-ray diffraction patterns of materials at deep discharge. The NMR results are also consistent with the relatively low Li occupancy of the Li octahedral (3b) site at 3.0 V (Table 1b); although the formation of the *m*-$LiMnO_2$ phase is associated with the 3.0 V peak in Figure 4, this phase clearly continues to grow following deeper discharging from 3.0 to 2.0 V. No evidence is seen for a resonance at 90−100 ppm due to octahedral Li sites in a spinel with the structure $Li_2Mn_2O_4$, consistent with the absence of such a tetragonal spinel in the diffraction data.

Extended Cycling. Considering first the electrochemical data, we see from Figure 4 that the overriding change is the emergence of a double 4 V process (2 pairs of redox peaks at 3.95 and 4.1 V), which is characteristic of spinel. It is also apparent, especially on examining the reduction peaks in the region of 4 V, that replacement of the splayered phase by spinel occurs as a two-phase process since the reduction peak at around 3.75 V diminishes in intensity as the two peaks at 3.95 and 4.1 V increase in intensity.

A series of cells was cycled for 5, 15, 25, 50, and 92 cycles. In each case cycling was arrested at 3.5 V on charging and material was extracted for neutron powder diffraction and Li NMR. Powder neutron diffraction patterns of these materials are shown in Figure 8. Considering first the 5-cycle data, possible structural models were explored using Rietveld refinement, and, as in the case of the data during the first cycle, a splayered structure provided a better fit to the data than was possible for a model based on a simple layered structure. Although the model with tetrahedral site occupancy provided a reasonable fit to the data, a further reduction in χ^2 of 33% was obtained by introducing a second phase with the structure of $LiMn_2O_4$ spinel. The two-phase refinement employed the usual splayered model within which occupancy on the 3a, 3b, and 6c sites were allowed to vary independently. The crystallographic parameters for the splayered phase are given in Table 2. It was not possible to simultaneously refine

(33) Grey, C. P.; Lee, Y. J. *Solid State Sci.* **2003**, *5*, 883.
(34) Pan, C.; Lee, Y. J.; Ammundsen, B.; Grey, C. P. *Chem. Mater.* **2002**, *14*, 2289.
(35) Lee, Y. J.; Grey, C. P. *J. Electrochem. Soc.* **2002**, *149*, A103.
(36) Lee, Y. J.; Grey, C. P. *J. Phys. Chem. B* **2002**, *106*, 3576.

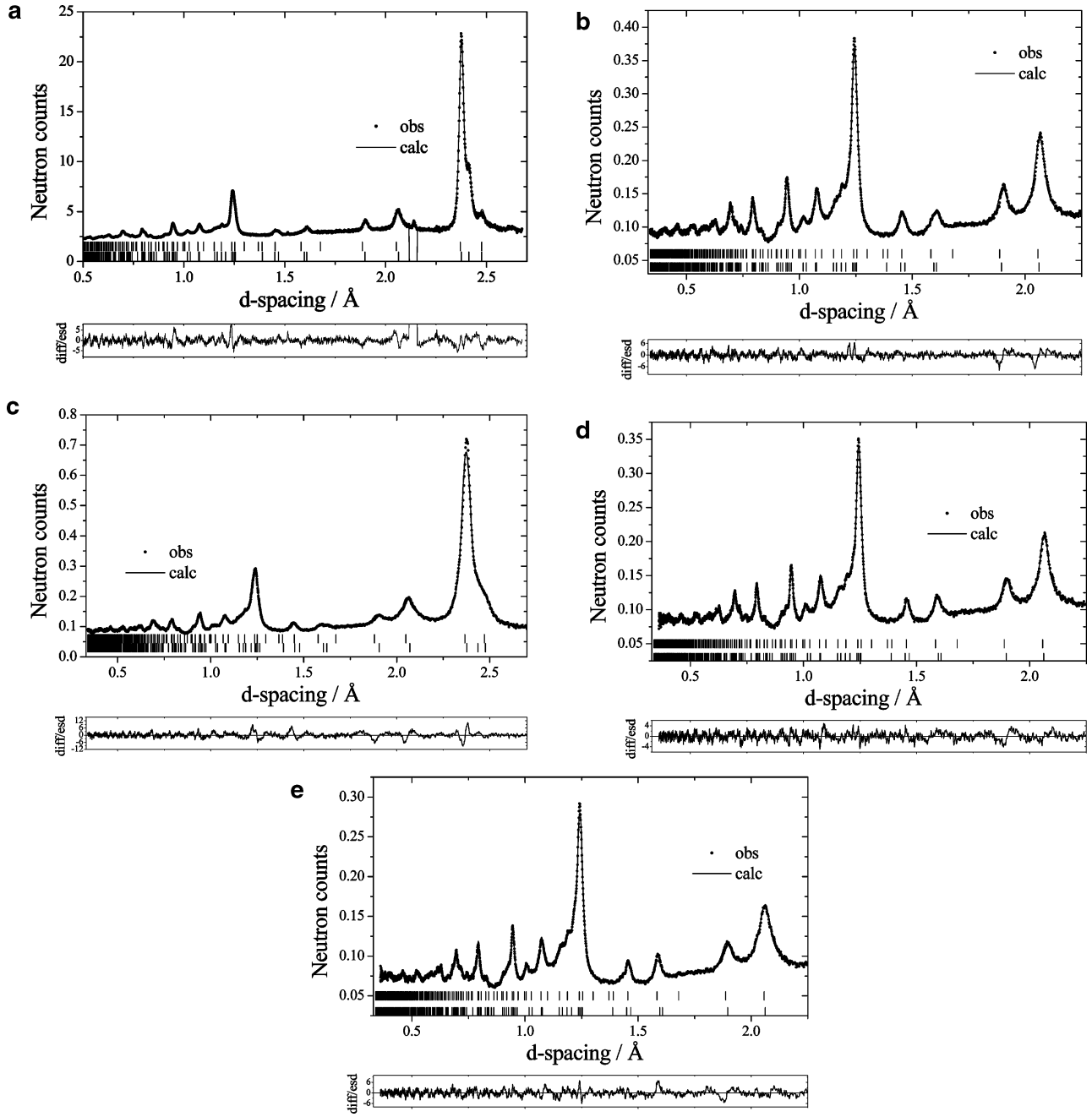

Figure 8. Refined powder neutron diffraction patterns for layered $LiMnO_2$ stopped at 3.5 V on charge. In each case the model contains splayered (lower tick marks) + spinel (upper tick marks) models. Dots represent observed data and the solid line represents the calculated pattern. The lower line is the difference/esd. (a) After 5 cycles; (b) after 15 cycles; (c) after 25 cycles; (d) after 50 cycles; and (e) after 92 cycles.

the structural parameters for the splayered and spinel phases, the latter were therefore fixed except for the lattice parameter which was observed to be close to that for stoichiometric spinel. This is in agreement with our previous observations which also indicated that the spinel obtained on cycling has a lattice parameter close to the stoichiometric material.[22] As a consequence, the model used for the spinel phase was that of regular spinel, i.e., $Li[8a]Mn_2[16d]O_4[32e]$. Considering the crystallographic data for the splayered phase we again note that the manganese occupancy of the 3a site is less than unity, consistent with the expected displacement of manganese in the splayered phase. As before, it is not possible to determine the degree to which the displaced manganese exists on the tetrahedral, 6c, or octahedral, 3b, sites; we describe the 6c and 3b sites as being occupied by lithium but recognize the coexistence of Li and Mn on one or both of these sites.

A similar two-phase model composed of splayered and spinel structures provided the best fit to the data at 15, 25. and 50 cycles. The fits are shown in Figure 8 and crystallographic data for cycle 15 are presented in Table 2. Again the structure of the spinel phase was fixed. The splayered phase remains broadly similar throughout, although there is evidence of increasing displacement of Mn from the octahedral 3a site in the manganese layers. This is to be expected as the material converts from a layered to a spinel structure. Note that after 92 cycles the proportion of splayered phase was too small to permit a meaningful refinement of the structural

Table 2. Refined Crystallographic Parameters for $LiMnO_2$ after (a) 5 Cycles, and (b) 15 Cycles, to 3.5 V on Charge; Fit to a Two-Phase Splayered + Spinel Model

atom	Wyckoff symbol	*x*/*a*	*y*/*b*	*z*/*c*	B_{iso}	occupancy
			(a) After 5 Cycles[a]			
Li1	3b	0	0	0.5	1.8(5)	0.41(5)
Li2	6c	0	0	0.119(2)	0.5(−)	0.23(1)
Mn1	3a	0	0	0	0.82(8)	0.94(2)
O1	6c	0	0	0.2613(2)	1.55(5)	1
			(b) After 15 Cycles[b]			
Li1	3b	0	0	0.5	1.0(−)	0.35(3)
Li2	6c	0	0	0.124(1)	0.5(−)	0.26(1)
Mn1	3a	0	0	0	0.94(12)	0.81(2)
O1	6c	0	0	0.2620(2)	1.57(6)	1

[a] $R_e = 0.77\%$, $R_{wP} = 1.16\%$, $R_P = 1.19\%$, $\chi^2 = 2.27$. Splayered phase. $a = 2.8998(9)$ Å, $c = 14.466(3)$ Å. Spinel phase, $a = 8.214(3)$ Å. Phase ratio 88:12. [b] $R_e = 1.47\%$, $R_{wP} = 2.36\%$, $R_P = 1.87\%$, $\chi^2 = 2.58$. Splayered phase. $a = 2.897(1)$ Å, $c = 14.470(4)$ Å. Spinel phase, $a = 8.226(3)$ Å. Phase ratio 77:23.

Table 3. Phase Fractions of Splayered and Spinel Obtained from Refinement of Neutron Diffraction Data, and Chemical Shift and Ratios of the Signals Attributed to the Layered Compound, the Intermediate, and the Spinel Obtained by Li NMR

Phase Fractions

	splayered	spinel
5 cycles	88%	12%
15 cycles	77%	23%
25 cycles	60%	40%
50 cycles	29%	71%
92 cycles	7%	93%

Chemical Shifts and Ratios

	layered		intermediate		spinel	
	shift (ppm)	ratio (%)	shifts (ppm)	ratios (%)	shifts (ppm)	ratios (%)
5 cycles	695	80	582	14	518	6
15 cycles	695	35	585	45	494	20
25 cycles	705	30	578	50	512	20
50 cycles	700	negligible	644	25	548	40
					483	35
92 cycles	700	negligible	612	25	546	35
					481	40

parameters. In this case the site occupancies were fixed at the values obtained from the refinement after 15 cycles. The proportions of layered to spinel material have been extracted from the refinements and are reported in Table 3. After 5 cycles only 12% of the material had converted to spinel, whereas at the end of 92 cycles this had risen to 93%. At 25 cycles around half the material had converted to spinel and this is in reasonable agreement with the electrochemical data in Figure 4 which, as mentioned above, clearly shows features of the splayered phase coexisting with spinel.

Li NMR data collected for each of the cycle numbers is shown in Figure 9. Three peaks are of particular importance in the spectra and are, in the case of the material after 5 cycles, apparent at approximately 695, 582, and 518 ppm. On the basis of our earlier work, the peak at 518 ppm is assigned to the spinel phase. The peak at 695 ppm is tentatively assigned to Li ions in a predominantly layered phase, based on the spectra observed in the first cycle. The position of the intermediate peak suggests that the Li^+ ion lies in an environment somewhere between that of the layered and spinel phases. The proportion of spinel peak grows slowly on

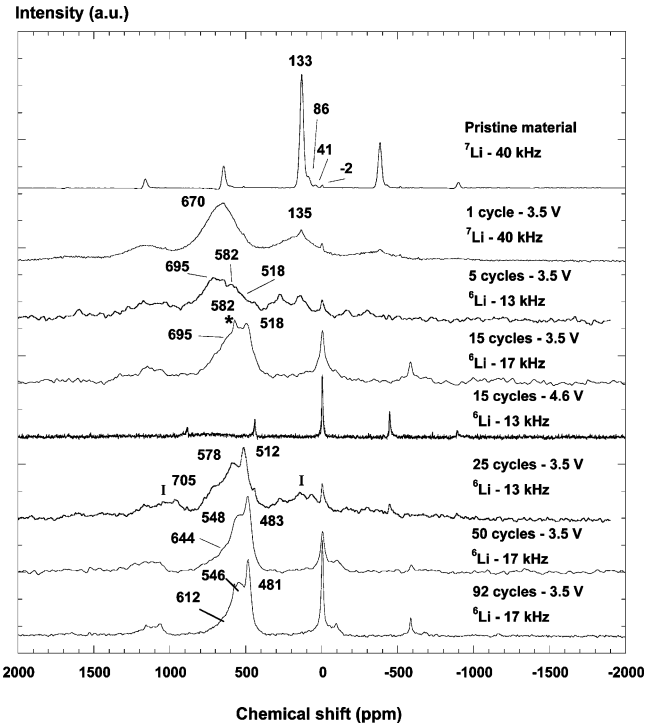

Figure 9. Lithium NMR as a function of cycle number, for samples charged to 3.5 V. The isotropic resonances are marked with their corresponding shifts; the remaining peaks are spinning sidebands. Note that the sideband of the electrolyte resonance overlaps with the resonances at 500−700 ppm for the ^6Li spectra acquired with a spinning frequency of 17 kHz, introducing an error into the intensities obtained from the deconvolution of these spectra. This sideband is marked with an "*" in the appropriate spectra; the sidebands of the intermediate phase are also marked with "I"s in the 25-cycle spectrum.

cycling and this is consistent with the neutron diffraction and electrochemical data in which we see the slow development of the double 4 V process. No clear evidence of the 518 ppm resonance is observed until we see the 4 V process (15 cycles). The spectrum for the 4.6 V material on the 15th cycle is dominated by the resonance due to diamagnetic Li on the surfaces of the particles, with the resonances at higher frequencies dropping noticeably in intensity. This indicates that the majority of the Li has been removed from the cathode and that the drop in capacity of these cathodes below the theoretical capacity is not associated with the inability to remove Li from these structures, but rather with the inability to reinsert Li in the potential range studied here.

Considering the origin of the intermediate peak at 582 ppm seen for the first 25 cycles, a similar resonance is observed for lithium-excess spinels such as $Li_{1.05}Mn_{1.95}O_4$ where it has been assigned to lithium ions in clusters of tetrahedral sites near Li^+ ions substituted into the octahedral sites of the spinel structure.[35] This resonance is associated with a characteristic resonance at approximately 2200 ppm, which can be detected even for the very disordered samples prepared at low temperatures (550 °C), by using ^7Li and very fast MAS.[33] ^7Li spectra of the material cycled 50 times showed no evidence of this local environment, indicating (a) that the spinels formed from the layered $LiMnO_2$ do not contain Li on the octahedral site of the spinel structure

and (b) that this is not the cause of the resonance at 582 ppm. ^{6}Li NMR spectra were acquired as a function of temperature up to 250 °C, to again confirm that the 582 ppm is not associated with octahedral lithium in the spinel structure. No coalescence of the resonances was observed at elevated temperatures, as is seen, for example, in $Li_{1.05}Mn_{1.95}O_4$.[35] The resonance assigned to the spinel phase grows in intensity, at the expense of the two other higher frequency resonances, as a function of heating time, and dominates the spectrum of the material after the sample was returned to room temperature, indicating that the two higher frequency resonances are due to metastable local environments. This conversion of the metastable layered $LiMnO_2$ phase to the thermodynamically stable spinel phase has been observed previously in our variable-temperature experiments on layered $LiMnO_2$.[30] This experiment again suggests that the resonance at 582 ppm is not associated directly with the spinel phase.

Moderately slow spinning frequency (13 kHz) ^{6}Li NMR data were acquired to probe the local environments of Mn surrounding the Li, since layered local environments are associated with characteristic (large) sidebands, while spinel environments are associated with smaller spinning sideband patterns.[36] Although the signal-to-noise ratios of these spectra are poor, the 582-ppm local environment contains larger, more intense spinning sidebands than those of the 518-ppm resonance. This can be seen most clearly for the first-order low-frequency sidebands in the 25-cycle ^{6}Li spectrum, where the sideband of the 578-ppm resonance is more intense than that of the 512-ppm resonance, even though the height of the sharper 512 ppm is much greater if the two isotropic resonances are compared. The width of the spinning sideband manifold appears to be intermediate between the layered and spinel resonances. The intermediate, 582-ppm, resonance cannot simply be associated with tetrahedral Li in the splayered phase, because the diffraction data show only a small increase in the tetrahedral site on cycling, whereas this NMR peak increases noticeably up to cycle number 25. Instead, the concentration of this resonance appears to be strongly correlated with the peak at 3.9 V seen in the incremental capacity plot (Figure 4), on reduction, which reaches a maximum after 25 cycles. We, therefore, associate this peak with the formation of spinel-like local (intermediate) environments still within the layered phase.

All three peaks move to lower resonance on extended cycling, with the shift being particularly noticeable when comparing the spectra of 25 and 50 cycles; the resonance at 700 ppm assigned to the layered phases essentially disappears. Broad, high-frequency resonances are seen at approximately 612 and 644 ppm in the spectra of 50 and 92 cycles. The incremental capacity plot now indicates that the spinel process is dominant for the 92-cycle sample. Presumably the local environments giving rise to the 582-ppm resonance in earlier cycles gradually order forming larger spinel nuclei, their resonances shifting to lower frequencies, leaving behind a residual disordered "intermediate" layered phase (612−644 ppm). Thus, the lower frequency resonances (at 546−481 ppm) are all assigned to spinel-type phases. The relative proportions of the 3

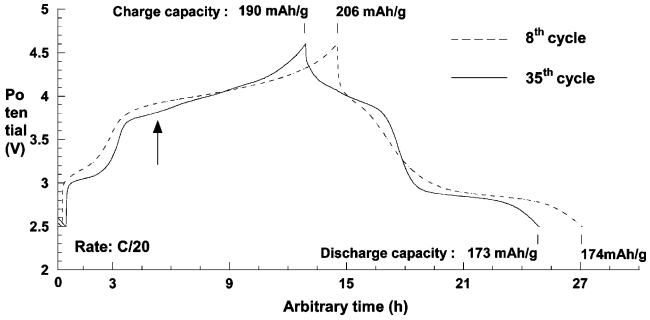

Figure 10. Charge and discharge curves for the 8th and 35th cycles obtained for the stoichiometric starting material by galvanostatic cycling at a typical rate of C/20.

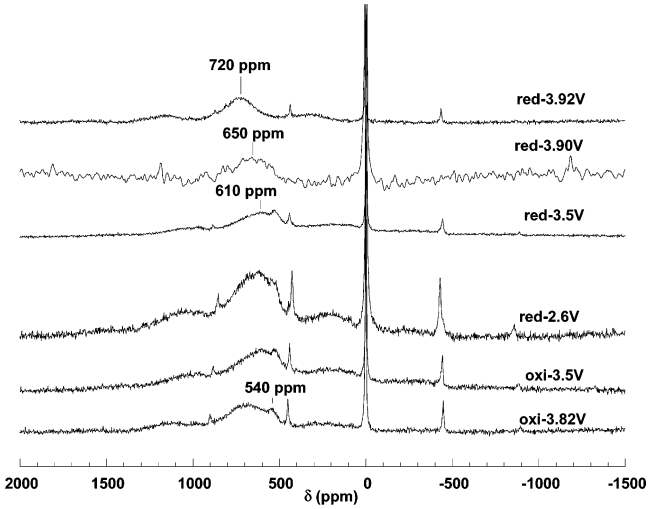

Figure 11. ^{6}Li MAS NMR spectra of cells stopped at different potentials during the 35th charge−discharge cycle. Spectra were acquired at spinning speeds of 13 kHz, except the spectrum of the 3.90 V sample which was obtained at 35 kHz.

peaks as a function of cycle number along with their assignments are shown in Table 3. Some care should be exercised when comparing the diffraction data and NMR data, since NMR measures the Li content in these phases which is not necessarily directly correlated with phase fraction. Despite this qualification, the two sets of data are in reasonable agreement.

To assign the different electrochemical processes observed in Figure 4 to changes in local environments, an additional series of cells was prepared, using ^{6}Li as the anode material (to improve the signal-to-noise of the spectra). The charge and discharge curves shown in Figure 10 show features similar to those seen in Figure 4. The processes at ∼3 and 4 V are evident as is the peak in Figure 4 at 3.9 V, which appears as an additional step in the charging curve on the 35th cycle (black arrow).

Detailed Analysis of the 35th. The spectra obtained after equilibrating different cells at different potentials in the 35th cycle are shown in Figure 11. The spectra obtained at 3.5 V on oxidation and reduction are qualitatively similar to those observed in the previous experiments although the resonances are much broader and the intensities of the resonances assigned to different local environments are quite different. For example, the peak assigned to an ordered spinel phase (515−540 ppm) is much less intense. These differences are ascribed to differences in the cycling conditions (a

lower cycling rate of C/20 was used to collect the data in Figure 10). The resonance at 610 ppm is again assigned to lithium in the intermediate phase and the resonance at 700 ppm is assigned to lithium in a layered manganese environment in the spectrum at 3.5 V. On lowering the potential to 2.6 V, no sign of a cooperative Jahn−Teller distortion is seen (no peak at either 100 ppm (tetragonal spinel $Li_2Mn_2O_4$) or 140 ppm (*m*-$LiMnO_2$)). The changes in intensities of the resonances are consistent with the Li intercalation levels calculated from the electrochemical data. For example, the total integrated intensity obtained for the 2.6 V spectrum is more than twice the integrated intensity for the 3.5 V sample, with the electrochemical data indicating that 0.6 and 1.3 Li^+ (based on the spinel formula, $Li_xMn_2O_4$) are intercalated at 3.5 and 2.6 V, respectively. Thus, the average manganese oxidation state in the 2.6 V sample is greater than 3 and Mn^{4+} ions are still present in this sample.

Surprisingly, the spectrum obtained following reduction to 3.92 V (i.e., after the two peaks in the incremental capacity plot attributed to the spinel phase or domains), does not contain the sharp approximately 520-ppm "spinel" resonance. The spinel resonance is only observed on further reduction to 3.5 V (i.e., after the 3.9 V reduction process seen in the incremental capacity plot). The spinel resonance is still present at 3.82 V on subsequent oxidation, indicating that the electrochemical process seen at 3.7 V on oxidation is not related to the 3.9 V reduction process. Instead, the 3.75 V oxidation process must be associated with the 3.0 V reduction process. This is consistent with the electrochemical data: The electrochemical reduction at 3.0 V on the 35th cycle involves approximately 0.68 Li^+ with respect to the $Li_xMn_2O_4$ formula (104 $mAhg^{-1}$), while the subsequent oxidation processes at 3.0 and 3.6 V involve, respectively, 0.32 Li^+ (49 $mAhg^{-1}$) and 0.31 Li^+ (48 $mAhg^{-1}$).

The spectrum obtained on reduction to 3.92 V contains only a very broad resonance centered at 720 ppm. The broad resonance shifts to lower frequencies (approximately 650 ppm) on lowering the potential to 3.90 V, as new sites are filled and the average manganese oxidation state decreases. A potential of 3.90 V corresponds to the tail end of the lower voltage (3.95 V) spinel process and is halfway through the 3.90 V process. This behavior is consistent with the spectra observed on charging $Li_{1.05}Mn_{1.95}O_4$, where the gradual shift of the tetrahedrally coordinated Li ions from 520 ppm to higher frequency was ascribed to an increase in the average oxidation state of the Mn ions in the first cation coordination sphere surrounding the tetrahedrally coordinated Li^+ ions.[35]

At the lower potentials (3.5 V), the broad resonance shifts further to 610 ppm and the "spinel" resonance is now seen. Thus, the 3.90 V reduction process and the tail end of the 3.95 V spinel peak appear to be associated with the formation of an ordered "spinel" peak and local environments with resonances at approximately 610 ppm. The 3.9 V peak process is associated with the broad resonance at 610 ppm, and it can be assigned to an intermediate environment due to a splayered phase, rather than the spinel phase. Both its shift and the voltage of process suggest that this environment is associated with tetrahedrally coordinated Li. The shift of the intermediate environment is consistent with those tabulated in Table 3b, for the samples cycled for more than 25 cycles. The 3.9 V peak must be buried under the "spinel" peaks on oxidation in Figure 4. Interestingly, peaks at 3.85 and 3.95 V were also observed on discharge, in extended cycling studies of orthorhombic $LiMnO_2$.[37]

Although some debate still remains in the literature as to the number of different phases formed on cycling the stoichiometric spinel $Li_{1-x}Mn_2O_4$,[24,40−41] the material is generally considered to comprise a solid solution region ($x = 0-0.5$) and a two-phase region. Since the 3.95 V process is associated with the continuous solid solution, its associated peak in the incremental capacity plot (Figure 4) is broader than the 4.05 V spinel peak, the process often continuing down to 3.8 V, depending on the exact cycling conditions. In our earlier NMR and diffraction study of this material a resonance was observed at 540 ppm on discharging corresponding to $Li_{0.9}Mn_2O_4$, and not until the samples were fully discharged to 3.5 V was the resonance at 518 ppm due to ordered $LiMn_2O_4$ observed.[24] Similarly, the resonance due to the ordered $Mn^{3.5+}$ spinel phase is not seen in this study until the sample has been discharged below the tail end of the 3.95 V spinel process. The larger concentration of the ordered "spinel" resonance in the samples prepared for neutron studies may be due to the fact that these samples were equilibrated for a much longer time before the data were collected. Because no evidence for substantial occupancy of the octahedral site by Li in the nucleated spinel phase is seen (by NMR or diffraction), the peaks seen at approximately 546−548 ppm in cycles 50 and 92 in Figure 9 and at slightly higher frequencies in earlier cycles (Figure 11) may be associated with Li ions near the "surfaces" of the small spinel domains, which may not be as well ordered as the Li in the centers of the growing spinel domains.

Effect of Cycling on the Low-Voltage Process. Figure 12 shows spectra of cathodes discharged to 2.5 or 2.6 V, prepared to explore the approximately 3 V processes. These NMR spectra were collected at fast spinning speeds to ensure that there is no overlap between the high and lower frequency resonances. The resonance at approximately 140 ppm due to the *m*-$LiMnO_2$ gradually disappears on cycling, and a very broad resonance, centered at approximately 490 ppm after 5 cycles and at 610 ppm after 8 cycles, grows in intensity. After 15 cycles, the 140 ppm resonance is still observed but is much weaker and a group of resonances at 530 (spinel), 610 (intermediate), and 720 ppm (layered) are now visible. At 35 cycles, no evidence for the 140 ppm resonance (*m*-$LiMnO_2$; 143 ppm) or the Jahn−Teller distorted spinel ($Li_2Mn_2O_4$; 90−110 ppm) is observed; the higher frequency resonances (at 530 ppm and above) dominate the spectra (spectra not shown). The spectrum at 2.6 V after 100 cycles contains a very

(37) Croguennec, L.; Deniard, P.; Brec, R. *J. Electrochem. Soc.* **1997**, *144*, 3323−3330.
(38) Tarascon, J.-M.; Guyomard, D. *J. Electrochem. Soc.* **1991**, *138*, 2864.
(39) Xia, Y.; Yoshio, M. *J. Electrochem. Soc.* **1996**, *143*, 825.
(40) Liu, W.; Kowal, K.; Farrington, G. C. *J. Electrochem. Soc.* **1998**, *145*, 459.
(41) Yang, X. Q.; Sun, X.; Lee, S. J.; McBreen, J.; Mukerjee, S.; Daroux, M. L.; Xing, X. K. *Electrochem. Solid-State Lett.* **1999**, *2*, 157.

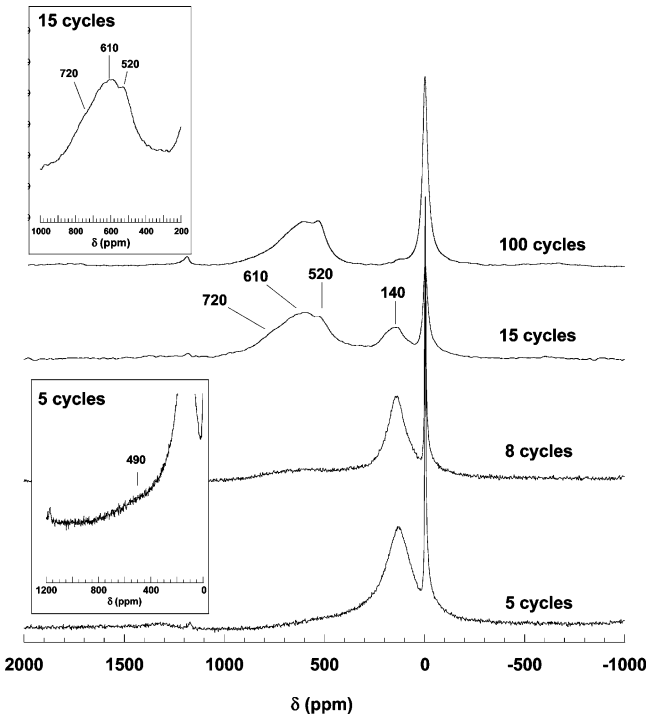

Figure 12. ^{6}Li MAS NMR spectra acquired with a spinning speed of 35 kHz, for cells discharged to 2.6 V after 5, 8, 15, and 100 charge−discharge cycles. Expansions of the 5 and 15 cycle spectra are shown.

weak peak with intensity of less than 1% of the total intensity at approx 100 ppm, which can be ascribed to a Jahn−Teller distorted phase, but again, higher frequency resonances at 530 and 603 ppm (and a higher frequency shoulder) dominate the spectra. Spin−lattice relaxation time (T_1) measurements were performed on a sample at 2.6 V after 8 cycles. The T_1s of the broad features at 547 and 650 ppm are approximately 30 ms, close to the typical value (40 ms) for lithium in the normal 8a position in ordered spinel (giving rise to a resonance at 520 ppm) and defect spinels (30 ms; 550−590 ppm). The resonance at 140 ppm is associated with a slightly longer T_1 time (50 ms), consistent with its assignment to the Jahn−Teller distorted phase. Thus, we ascribe the oxidation process at 3.15 V seen clearly in Figure 4 in the early cycles (5−50) to the removal of octahedral Li ions (oct-Li) in a layered, Jahn−Teller distorted phase. The lower voltage peak seen in later cycles (>15) at 3.05 V is then ascribed to the removal of oct-Li from a non-Jahn−Teller distorted splayered phase or spinel-like domain in the material. The small shoulder seen at higher voltages on the 3.0 V process at 100 cycles is ascribed to the very small regions of the sample that undergo a Jahn−Teller distortion and give rise to the weaker resonances at approximately 100 ppm.

The mechanism by which Li is deintercalated from the non-Jahn−Teller distorted phases is more complicated. Comparing the spectra at 2.6 V and 3.5 V after 35 cycles, the removal of the first set of octahedral Li ions at approximately 3.05 V is associated with a decrease in ^{6}Li intensity of a very broad resonance at around 500−700 ppm. However, as discussed above, this oxidation step is associated with less Li removal than the insertion process that occurs at a similar voltage on discharge (Figure 10), and the insertion process is associated with both the 3.0 and 3.75 V oxidation steps. The 3.75 V oxidation process (Figure 4) grows steadily on cycling, reaching a maximum at 25−50 cycles, decreasing thereafter, consistent with its assignment to Li removal from the intermediate domains or local environments. This process is associated with a decrease in intensity centered around 630 ppm and a noticeable increase in the relative concentration of the resonance at approximately 700 ppm, the shift of the Li resonance being ascribed in part to an increase in the oxidation state of the manganese ions near the residual Li (octahedral and tetrahedral) ions and/or an increase in Li coordination number in the intermediate phase. The shift of the resonance near 630 ppm is consistent with the removal of either tetrahedral Li ions near manganese ions with an average oxidation state of >3.5+, or octahedral Li ions in environments with Mn vacancies nearby. The former suggestion appears to contradict the observation of a second higher voltage (seen more clearly on reduction) process for the intermediate phase. The voltage of the process is also not consistent with the simple removal of octahedral Li ions. However, insertion of Li into this phase does occur below 3.0 V, which is consistent with a process involving oct-Li. This deintercalation/intercalation is associated with a very large hysteresis or activation energy suggesting it involves cation migrations or structural rearrangements. Thus, we tentatively assign this process to the removal of octahedral Li ions, and simultaneous migration of cations within the structure (e.g., migration of Mn ions from a Mn *layer*, to a Mn tetrahedral site). In the first stages of cycling (cycles 1−15), this process is even less well defined and may occur at higher voltages, increasing the concentration of octahedral Li ions that are present at 3.5 V, even though they might be expected to have been removed already at this potential.

Implications and Summary. Reed et al. have noted that the formation of tetrahedral Li and Mn is relatively easy, whereas the reorganization of the ions to form the spinel phase is somewhat more difficult.[32] They also suggest that formation of a discrete spinel phase is preceded by the tetrahedral cations coming together within the splayered phase to form a structure closer to that of spinel. In other words the cation arrangement although still a layered structure will now resemble fragments of spinel. We postulate that the peak at intermediate shift in the NMR data arises from lithium in this intermediate state. This is consistent with the rise then fall in the proportion of the intermediate peak as the concentration of the intermediate state increases on cycling and then diminishes to be replaced by the fully ordered spinel. This explanation is also consistent with the electrochemistry, Figure 4, the peaks at 3.75 V on oxidation and at around 3.9 V on the discharge cycle (which are assigned to processes involving octahedral and tetrahedral Li, respectively) reaching a maximum in intensity at around 25−50 cycles and thereafter diminishing slowly. It may also be noted that a peak at a similar voltage has been observed in other spinel systems, most notably the so-called low-temperature spinel which has been described as a structure somewhat intermediate between a regular layered and a spinel phase.[38] Although the diffraction data after 92 cycles are dominated by a regular spinel phase with

little splayered material, the NMR data suggest that the intermediate and even the splayered structures still exist. This of course is a reflection of the fact that the NMR data probe the short-range structure and therefore can identify the persistence of disordered materials that are not evident in the diffraction data.

It is now possible to summarize the changes which accompany the transformation of layered $LiMnO_2$ to the spinel structure. On first extracting Li from $LiMnO_2$, Jahn−Teller inactive Mn^{4+} forms. As a result of the rapid mobility of the Li^+ ions and the electrons, segregation into regions of undistorted $Li_{0.5}MnO_2$ of $R\bar{3}m$ symmetry and regions of Jahn−Teller distorted $LiMnO_2$ of $C2/m$ symmetry provides an energetically feasible way of accommodating the mixture of Jahn−Teller active Mn^{3+} and inactive Mn^{4+}. The two phases coexist within the composition range $Li_{0.5}MnO_2$ to $LiMnO_2$ and with gradual replacement of the latter by the former as lithium continues to be extracted. $Li_{0.5}MnO_2$ has the spinel composition. As soon as $Li_{0.5}MnO_2$ forms, Mn ions migrate from their octahedral sites in the Mn layers through a shared face into an empty tetrahedral site located in the Li layers. The Li ions in the alkali metal layers will avoid the octahedral sites which share faces with this tetrahedral site in order to minimize repulsions. The displacement of these Mn ions also makes it possible for Li to move from the octahedral to tetrahedral sites within the Li layers; this was not previously possible because such sites shared faces with the Mn ions in octahedral sites in the Mn layers. As a result of these changes we clearly observe Li/Mn ions in tetrahedral sites within a layered structure by diffraction, i.e., formation of a splayered phase. As more lithium is removed, the composition drops below $Li_{0.5}MnO_2$ and lithium ions are extracted from the structure at 4 V. Considerable structural reorganization is taking place at this stage and we associate the 4 V peak in the first 15 cycles with this rather than extraction of Li from tetrahedral sites per se, since both octahedral and tetrahedral Li persist at this point. On discharge, not all the lithium is returned at this voltage further confirming that significant structural reorganization is taking place. Subsequent cycling reveals that the splayered phase persists and does not change substantially in composition, but gradually transforms to spinel. However, it would appear that this process occurs through an intermediate structure with many features common to spinel. This intermediate local environment or domain increases in proportion up to cycle number 25 and may be associated with the oxidation peak at 3.75 V (oct-Li) and the 3.9 V reduction peak (tet-Li) seen in Figure 4, as well as accounting for the intermediate peak in the NMR data. Octahedral Li are present, even at 3.5 V (diffraction data), consistent with these proposals. As cycling continues, long range ordered spinel forms and is evident in the diffraction and NMR data. Ultimately, on extended cycling the entire structure forms a relatively well ordered crystalline spinel phase. The domain size and/or residual defects of this spinel do not allow the cooperative Jahn−Teller distortion to occur.

Acknowledgment. P.G.B. thanks the Royal Society and EPSRC for funding. C.P.G. thanks the NSF (grant DMR0211353) and the Dreyfus Foundation for support (through a Camille and Henry Teacher Scholar Award to C.P.G.).

CM034964B